

**Journal of Atmospheric and Oceanic Technology**  
**Turbulence Measurements from Compliant Moorings - Part II: Motion Correction**  
--Manuscript Draft--

<b>Manuscript Number:</b>	
<b>Full Title:</b>	Turbulence Measurements from Compliant Moorings - Part II: Motion Correction
<b>Article Type:</b>	Article
<b>Corresponding Author:</b>	Levi Farenorth Kilcher, Ph.D. National Renewable Energy Lab Golden, Colorado UNITED STATES
<b>Corresponding Author's Institution:</b>	National Renewable Energy Lab
<b>First Author:</b>	Levi Farenorth Kilcher, Ph.D.
<b>Order of Authors:</b>	Levi Farenorth Kilcher, Ph.D.  Jim Thomson, Ph.D.  Samuel Harding, Ph.D.  Sven Nylund
<b>Abstract:</b>	Acoustic Doppler velocimeters (ADVs) are a valuable tool for making high-precision measurements of turbulence, and moorings are a convenient and ubiquitous platform for making many kinds of measurements in the ocean. However---because of concerns that mooring motion can contaminate turbulence measurements and acoustic Doppler profilers are relatively easy to deploy---ADVs are not frequently deployed from moorings. This work details a method for measuring turbulence using moored ADVs that corrects for mooring motion using measurements from inertial motion sensors. Three distinct mooring platforms were deployed in a tidal channel with inertial-motion-sensor-equipped ADVs. In each case, the motion correction based on the inertial measurements dramatically reduced contamination from mooring motion. The spectra from these measurements have a shape that is consistent with other measurements in tidal channels, and have a $f^{-5/3}$ slope at high frequencies---consistent with Kolmogorov's theory of isotropic turbulence. Motion correction also improves estimates of cross-spectra and Reynold's stresses. Comparison of turbulence dissipation with flow speed and turbulence production indicates a bottom boundary layer production-dissipation balance during ebb and flood that is consistent with the strong tidal forcing at the site. These results indicate that inertial-motion-sensor-equipped ADVs are a valuable new tool for measuring turbulence from moorings.
<b>Suggested Reviewers:</b>	Jonathan Nash, Ph.D. Professor, Oregon State University nash@coas.oregonstate.edu Expert in oceanic turbulence measurements.  Jim VanZwieten, Ph.D. Professor, Florida Atlantic University jvanzwi@fau.edu Experience with the instruments and data presented.  Natasha Lucas, Ph.D. Bangor University oss01c@bangor.ac.uk Expert in ocean turbulence, and has expressed interest in this work.  Ilker Fer, Ph.D. University of Bergen ilker.fer@gfi.uib.no Experience with similar instrumentation.  Jeremy Kasper, Ph.D. Assistant Professor, University of Alaska Fairbanks jkasper@alaska.edu

Experience with instrumentation, and an expressed interest in the methods.

Scott Miller, Ph.D.

Research Associate, State University of New York at Albany

[smiller@albany.edu](mailto:smiller@albany.edu)

Expert in similar methods and instrumentation in the atmosphere.



Friday, October 28, 2016

***Journal of Atmospheric and Oceanic Technology***

Dear Editor,

I am pleased to submit the paper entitled “Turbulence measurements from compliant moorings - Part II: motion correction” to the Journal of Atmospheric and Oceanic Technology.

High-fidelity measurements of turbulence in the ocean have long been challenging to collect, in particular in the middle of the water column. The work presented in this submission addresses this technology gap by presenting a method for motion correcting moored Acoustic Doppler Velocimeter (ADV) measurements. I believe the methods, data, and technology presented herein have applications both for fundamental studies of turbulence dynamics (e.g., energy cascades) and for engineering of marine structures (e.g., fatigue loads of tidal turbines). Perhaps most importantly, these new measurement techniques will enable improved validation of numerical simulations.

The research presented in this submission represents the second part of a two part publication submitted to the Journal of Atmospheric and Oceanic Technology, with the work divided as follows:

- . 1) Turbulence measurements from compliant moorings - Part I: motion characterization This article presents a range of compliant mooring platforms tested in energetic tidal sites for the application of mid-water turbulence measurements. The motion at the ADV location is characterized for each platform configuration to inform the most stable designs to meet particular deployment objectives.
- . 2) Turbulence measurements from compliant moorings - Part II: motion correction This article describes the methods used to isolate the true velocity fluctuations of turbulent flows from the inherent motion of compliant moorings. Higher order velocity statistics are compared with turbulence theory and other turbulence measurements to validate the techniques presented.

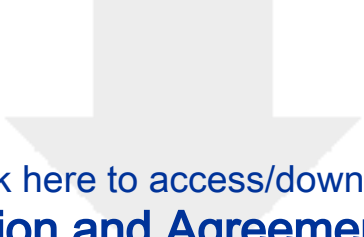
Part 1 was submitted late last month; I apologize it has taken me this long to send you this second part. The corresponding author for this article is Dr. Levi Kilcher, and is coauthored by Dr. Jim Thomson of the Applied Physics Laboratory at the University of Washington, Dr. Sam Harding at the Pacific Northwest National Lab, and Sven Nylund, of Nortek AS. Please send any communication concerning this paper by email to [samuel.harding@pnnl.gov](mailto:samuel.harding@pnnl.gov).

Thank you in advance for considering this submission and I look forward to hearing from you.

Sincerely,

Dr. Levi Kilcher

Engineer IV – Water Power  
National Renewable Energy Lab  
Email: [levi.kilcher@nrel.gov](mailto:levi.kilcher@nrel.gov)  
Tel: (303) 384-7192



Click here to access/download

**Cost Estimation and Agreement Worksheet**  
**Cost Estimation and Agreement Worksheet\_filled.pdf**

# Turbulence Measurements from Compliant Moorings - Part II: Motion

<sup>3</sup> Levi Kilcher\*, Jim Thomson, Samuel Harding, and Sven Nylund

<sup>4</sup> \*Corresponding author address: National Renewable Energy Laboratory, Golden, Colorado

<sup>5</sup> E-mail: Levi.Kilcher@nrel.gov

## ABSTRACT

6 Acoustic Doppler velocimeters (ADVs) are a valuable tool for making high-  
7 precision measurements of turbulence, and moorings are a convenient and  
8 ubiquitous platform for making many kinds of measurements in the ocean.  
9 However—because of concerns that mooring motion can contaminate tur-  
10 bulence measurements and acoustic Doppler profilers are relatively easy to  
11 deploy—ADVs are not frequently deployed from moorings. This work de-  
12 tails a method for measuring turbulence using moored ADVs that corrects  
13 for mooring motion using measurements from inertial motion sensors. Three  
14 distinct mooring platforms were deployed in a tidal channel with inertial-  
15 motion-sensor-equipped ADVs. In each case, the motion correction based on  
16 the inertial measurements dramatically reduced contamination from mooring  
17 motion. The spectra from these measurements have a shape that is consistent  
18 with other measurements in tidal channels, and have a  $f^{-5/3}$  slope at high  
19 frequencies—consistent with Kolmogorov’s theory of isotropic turbulence.  
20 Motion correction also improves estimates of cross-spectra and Reynold’s  
21 stresses. Comparison of turbulence dissipation with flow speed and turbu-  
22 lence production indicates a bottom boundary layer production-dissipation  
23 balance during ebb and flood that is consistent with the strong tidal forcing  
24 at the site. These results indicate that inertial-motion-sensor-equipped ADVs  
25 are a valuable new tool for measuring turbulence from moorings.

26 **1. Introduction**

27 Acoustic Doppler velocimeters (ADVs) have been used to make high-precision measurements of  
28 water velocity for over 20 years (Kraus et al. 1994; Lohrmann et al. 1995). During that time, they  
29 have been deployed around the world to measure turbulence from a range of platforms, including  
30 stationary structures on ocean- and lake-bottoms, in surface waters from a pole lowered from  
31 a ship's bow, and in the deep ocean from autonomous underwater vehicles (e.g., Voulgaris and  
32 Trowbridge 1998; Zhang et al. 2001; Kim et al. 2000; Goodman et al. 2006; Lorke 2007; Geyer  
33 et al. 2008; Cartwright et al. 2009).

34 A relatively small fraction of ADV measurements have been made from moorings (e.g., Fer  
35 and Paskyabi 2014). Presumably this is because mooring motion can contaminate ADV mea-  
36 surements, and acoustic Doppler profilers (ADPs) can be used to measure mid-depth turbulence  
37 statistics without a mooring (e.g., Stacey et al. 1999a; Rippeth et al. 2002; Wiles et al. 2006).  
38 Still, ADV measurements have distinct characteristics that can be advantageous: they are capa-  
39 ble of higher sample rates, have higher signal-to-noise ratios, and have a much smaller sample  
40 volume (1 centimeter, as opposed to several meters). That is, compared to an ADP, ADVs are  
41 high-precision instruments capable of providing unique information. They could be more widely  
42 used as a moored instrument (i.e., at an arbitrary depth) if a method for accounting for mooring  
43 motion can be demonstrated to provide more accurate estimates of turbulence statistics.

44 Inertial motion unit (IMU) sensors have been used in the aerospace and aeronautical industries  
45 to quantify the motion of a wide range of systems for several decades (Bevly 2004). Over the  
46 last 10 years, the smartphone, drone, and ‘Internet of Things’ markets has driven innovation in  
47 microelectrical-mechanical systems, including the IMU. As a result of this growth and innovation  
48 the cost, power requirements, and size of IMUs have come down. Also known as MARG (mag-

49 netic, angular-rate, gravity), or AHRS (attitude heading reference system) sensors, IMUs measure  
50 three axes of the Earth’s magnetic field, angular rotation, and linear acceleration.<sup>1</sup> These sig-  
51 nals are then integrated using Kalman filters to estimate the orientation and motion of the sensor  
52 (Barshan and Durrant-Whyte 1995; Marins et al. 2001; Bachmann et al. 2003).

53 Nortek now offers a version of their Vector ADV with a Microstrain 3DM-GX3-25 IMU sensor  
54 (Nortek 2005; MicroStrain 2012). The IMU’s signals are incorporated into the Vector data stream  
55 so that the motion and orientation signals are tightly synchronized with the ADV’s velocity mea-  
56 surements. This tight synchronization provides a data stream that can be utilized to quantify ADV  
57 motion in the Earth’s inertial reference frame, and remove that motion from the ADV’s velocity  
58 measurements at each time step of its sampling. This work specifies a method for performing  
59 motion correction of these ‘ADV-IMU’ measurements, and presents results of this method using  
60 data from a range of mooring configurations that positioned ADV-IMUs at mid-depths in Puget  
61 Sound.

62 This effort was originally motivated by a need for low-cost, high-precision turbulence measure-  
63 ments for the emerging tidal energy industry (McCaffrey et al. 2015; Alexander and Hamlington  
64 2015). Experience in the wind energy industry has shown that wind turbine lifetime is reduced by  
65 atmospheric turbulence, and the same is expected to be true for tidal energy turbines. In wind, me-  
66 teorological towers are often used to position sonic anemometers at the hub height of wind turbines  
67 for measuring detailed turbulence inflow statistics (Hand et al. 2003; Kelley et al. 2005; Mücke  
68 et al. 2011; Afgan et al. 2013). In the ocean, tower-mounted hub-height turbulence measurements  
69 have been made, but they are challenging to install and maintain in energetic tidal sites (Gunawan  
70 et al. 2014; Thomson et al. 2012). Therefore, the U.S. Department of Energy funded this work to

---

<sup>1</sup>Within this literature, IMU is generally reserved for a MARG sensor without a magnetometer, but herein we refer to the entire group of sensors that measure motion using accelerometers and angular-rate sensors as IMUs.

71 investigate the accuracy of mooring-deployed ADV-IMUs to reduce the cost of turbulence mea-  
72 surements at tidal energy sites (Kilcher et al. 2016). The approach proved to be successful and  
73 potentially useful to the broader oceanographic community interested in moored turbulence mea-  
74 surements (Lueck and Huang 1999; Doherty et al. 1999; Nash et al. 2004; Moum and Nash 2009;  
75 Alford 2010; Paskyabi and Fer 2013).

76 The next section describes details of the measurements, including a summary of the hardware  
77 configurations (platforms) that were used to support and position the ADV-IMUs in the water  
78 column. A detailed description of the motion of these platforms is found in the companion paper to  
79 this work, Harding et al. (in review), hereafter Part 1. Section 3 describes the mathematical details  
80 of motion correction and Section 4 presents results from applying the method to measurements  
81 from the various platforms. Section 5 is a discussion of the energetics of the tidal channel in  
82 which the measurements were made and demonstrates that the measurements are consistent with  
83 turbulence theory and other measurements in similar regimes. A summary and concluding remarks  
84 are provided in Section 6.

## 85 **2. Measurements**

86 This work focuses on measuring turbulence from ADVs that are deployed from nonstationary  
87 platforms and equipped with IMUs. The ADVs utilized for these measurements were equipped  
88 with Microstrain 3DM-GX3-25 IMU sensors that captured all six components of the ADV mo-  
89 tion (three components of angular rotation and three components of linear acceleration), as well  
90 as the orientation of the ADV pressure case. The sampling of the motion sensor is tightly syn-  
91 chronized with the ADV measurements. The IMU measures its motion at 1 kHz and uses internal  
92 signal integration (Kalman filtering) to output the motion signals at the same sample rate as the  
93 ADV's velocity measurements. This reduces aliasing of the IMU's motion measurements above

<sup>94</sup> the ADV's sample rate (MicroStrain 2010). Cable-head ADVs were used throughout this work to  
<sup>95</sup> allow for flexibility in the positioning of the ADV head relative to its pressure case.

<sup>96</sup> All measurements used in this work were made in Admiralty Inlet, Washington, approximately  
<sup>97</sup> 500 m west southwest of Admiralty Head in 60-m of water near  $48^{\circ} 9.18' N$ ,  $122^{\circ} 41.22' W$   
<sup>98</sup> (Figure 1). The site is approximately 6 km east of Port Townsend, and 1 km north of the Port  
<sup>99</sup> Townsend to Coupeville ferry route. Admiralty inlet is the largest waterway connecting Puget  
<sup>100</sup> Sound to the Strait of Juan de Fuca, and it possesses a large semidiurnal tidal flow (Thomson  
<sup>101</sup> et al. 2012; Polagye and Thomson 2013). This work utilizes data from three distinct deployment  
<sup>102</sup> platforms: the tidal turbulence mooring, a StableMoor buoy, and a simple sounding weight. All  
<sup>103</sup> data used in this analysis is available from the MHK data repository (<http://mhkdr.openei.org>;  
<sup>104</sup> submission ids: 49, 50 and 51). Additional details, photos, and schematic diagrams of all three  
<sup>105</sup> mooring systems can be found in Part 1.

<sup>106</sup> *a. Tidal Turbulence Mooring*

<sup>107</sup> The tidal turbulence mooring (TTM) is a simple mooring system with a strongback fin sus-  
<sup>108</sup> pended between a steel clump-weight anchor weighing 1,200 kg when dry and a 0.93-m-diameter  
<sup>109</sup> spherical steel buoy with a buoyancy of 320 kg. The ADV pressure cases were clamped to one  
<sup>110</sup> side of the strongback fin and the ADV sensor head was positioned 10 cm in front of the fin's  
<sup>111</sup> leading edge (Figure 2). The leading edge of the fin is fastened inline with the mooring line. This  
<sup>112</sup> configuration was designed to work like a weather vane, such that the drag on the fin held the ADV  
<sup>113</sup> head upstream of the mooring components. This work utilizes data from two TTM deployments.

<sup>114</sup> 1) JUNE 2012 TTM DEPLOYMENT

<sup>115</sup> The first TTM deployment was in June 2012 from 17:30 on the 12th until 14:30 on the 14th  
<sup>116</sup> (local; i.e., Pacific Daylight Time). Two Nortek ADVs were clamped to either side of the fin so that  
<sup>117</sup> the axis of their cylindrical pressure cases were parallel with the leading edge of the strongback.  
<sup>118</sup> The ADV heads were spaced 0.5 m apart vertically along the fin. Only one of these ADVs was  
<sup>119</sup> equipped with an integrated IMU. This TTM also had an upward-looking acoustic Doppler profiler  
<sup>120</sup> mounted on the mooring anchor.

<sup>121</sup> Periods of time during which this mooring interfered with a beam of the Doppler profiler were  
<sup>122</sup> identified by inspecting the profiler's acoustic amplitude signal. Periods during which one beam  
<sup>123</sup> of the profiler had  $> 5\%$  higher acoustic amplitude than the other beams were flagged as "contam-  
<sup>124</sup> inated" and excluded from averaging. Five-minute averages in which more than 50% of the data  
<sup>125</sup> were contaminated in this way were masked as invalid.

<sup>126</sup> 2) JUNE 2014 TTM DEPLOYMENT

<sup>127</sup> The second TTM deployment was in 2014 from 06:00 on June 17 to 05:00 on June 19 (local  
<sup>128</sup> time). Two Nortek ADV-IMUs were mounted on this TTM, with their heads spaced 0.5 m apart  
<sup>129</sup> along the fin. In this case, the pressure cases and ADV heads were inclined at an angle of 18° to  
<sup>130</sup> the leading edge of the fin to account for mooring blowdown during strong currents (Figure 3).  
<sup>131</sup> This change was made to reduce vibrational motion observed during the June 2012 deployment  
<sup>132</sup> that was believed to be associated with the orientation of the pressure cases.

<sup>133</sup> b. *The StableMoor platform*

<sup>134</sup> The second deployment platform was a cylindrical, StableMoor, syntactic foam buoy (manufac-  
<sup>135</sup> turer: Deep Water Buoyancy) that was anchored to a clump weight that weighed 2,700 lbs (Figure

<sup>136</sup> 4). The buoy is 3.5 m long and 0.45 m in diameter with a tail ring that is 0.76 m in diameter. The  
<sup>137</sup> StableMoor buoy weighs 295 kg in air, and has a buoyancy of 185 kg in water.

<sup>138</sup> The StableMoor buoy was deployed with an ADV-IMU mounted at its nose from 11:21 on May  
<sup>139</sup> 12 to 11:53 on May 13, 2015 (local time). The sample volume of the ADV is 10 cm forward of  
<sup>140</sup> the nose and 20 cm above the center line of the StableMoor buoy (Figure 4). Based on Wyngaard  
<sup>141</sup> et al.'s (1985) investigation of a similarly shaped slender body, the velocity measurements should  
<sup>142</sup> have flow-distortion effects of less than 10%. This configuration was designed to be the most  
<sup>143</sup> stable platform for measuring turbulence from a moving platform. The StableMoor buoy was  
<sup>144</sup> equipped with a 1,200-kHz RDI workhorse sentinel acoustic Doppler profiler that was oriented  
<sup>145</sup> downward-looking to measure water velocity below the platform in twelve 1-m bins and measure  
<sup>146</sup> buoy motion ("bottom tracking"), all at a 1-Hz sample rate.

<sup>147</sup> The buoy was ballasted to pitch upward a few degrees in zero-flow to avoid "flying downward."  
<sup>148</sup> In the presence of an oncoming current, the tail fins help to orient it into the flow. The anchor for  
<sup>149</sup> this buoy is similar to that of the TTM, including an acoustic release so the mooring and anchor  
<sup>150</sup> can be recovered separately.

<sup>151</sup> The StableMoor platform has two primary advantages compared to the TTM. First, it is signif-  
<sup>152</sup> icantly more massive and hydrodynamically stable than the TTM, which reduces the frequency  
<sup>153</sup> of motions of the platform. Second, the StableMoor platform is capable of supporting a bottom-  
<sup>154</sup> tracking acoustic Doppler profiler, which provides an independent measure of the platform's trans-  
<sup>155</sup> lational motion. Disadvantages of the StableMoor include: its size, which adds to the challenge of  
<sup>156</sup> deployment and recovery, and its cost, which is significantly higher than the TTM system.

157 *c. Turbulence Torpedo*

158 The turbulence torpedo is a simple sounding weight with an ADV head mounted forward of the  
159 nose, and the ADV pressure case strapped below. This platform was deployed on May 14, 2015,  
160 for 37 minutes starting at 07:41 local time. This measurement was made from a davit that hung  
161 the system from the side of the ship to a depth of approximately 25 m. The primary logistical  
162 advantages of this platform are its compact size, low cost, and the flexibility to perform spatial  
163 transects.

164 *d. Coordinate system and turbulence averaging*

165 Unless stated otherwise, vector quantities in this work are in a fixed “principal-axes” coordinate  
166 system that is aligned with the bidirectional tidal flow: positive  $u$  is in the direction of ebb ( $310^\circ$   
167 True), positive  $w$  is vertically upward, and  $v$  is the cross-stream component in a right-handed  
168 coordinate system. The full velocity vector,  $\vec{u} = (\tilde{u}, \tilde{v}, \tilde{w})$ , is separated into a mean and turbulent  
169 component as  $\vec{\tilde{u}} = \vec{\bar{u}} + \vec{u}$ , where the over-bar denotes a 5-minute average. Turbulence kinetic  
170 energy,  $tke = \overline{u^2} + \overline{v^2} + \overline{w^2}$ , and Reynold’s stresses,  $\overline{uv}$ ,  $\overline{uw}$ ,  $\overline{vw}$ , are computed by averaging over the  
171 5-minute window. Throughout this work, we use  $\bar{U} = (\bar{u}^2 + \bar{v}^2)^{1/2}$  to denote the mean horizontal  
172 velocity magnitude.

173 All spectra,  $S\{x\}(f) = |\mathcal{F}\{x(t)\}|^2$ , and cross spectra,  $C\{x,y\}(f) = \text{real}(\mathcal{F}\{x(t)\}\mathcal{F}\{y(t)\})$ , are  
174 computed using NumPy fast Fourier transform routines (van der Walt et al. 2011). Here,  $\mathcal{F}\{x(t)\}$   
175 denotes the fast Fourier transform of a signal  $x(t)$ . Time series, e.g.,  $x(t)$ , are linearly detrended  
176 and Hanning windowed prior to computing  $\mathcal{F}\{x\}$  to reduce spectral reddening.

177 Throughout the remainder of this work, the dependence of  $S$  and  $C$  on  $f$  is implied (e.g.,  $S\{x\}(f)$   
178 is hereafter  $S\{x\}$ ), and for other variables the dependence on  $t$  is implied. Spectra and cross  
179 spectra are normalized to preserve variance:  $\int S\{u\}df = \overline{u^2}$ , and  $\int C\{u,v\}df = \overline{uv}$ . The notations

<sup>180</sup>  $S\{\vec{u}\} = (S\{u\}, S\{v\}, S\{w\})$ , and  $C\{\vec{u}\} = (C\{u, v\}, C\{u, w\}, C\{v, w\})$  denote the set of spectra and  
<sup>181</sup> cross spectra for each velocity component and pairs of components, respectively.

<sup>182</sup> Turbulence dissipation rates are computed as:

$$\epsilon = \frac{1}{\bar{U}} \left( \alpha \left\langle (S\{u\} + S\{v\} + S\{w\}) f^{5/3} \right\rangle_{f_{IS}} \right)^{3/2} \quad (1)$$

<sup>183</sup> Where  $\alpha = 0.5$ , and  $\langle \rangle_{f_{IS}}$  denotes an average over the inertial subrange of the velocity spectra and  
<sup>184</sup> where the signal-to-noise ratio is small (Lumley and Terray 1983; Sreenivasan 1995). Throughout  
<sup>185</sup> this work, we take this average from 0.3 to 1 Hz for the  $u$  and  $v$  components, and 0.3 to 3 Hz for  
<sup>186</sup> the  $w$  component.

### <sup>187</sup> 3. Methodology

<sup>188</sup> The essential approach of motion correction is to estimate the time series of velocity on a com-  
<sup>189</sup> pliant mooring by obtaining an independent estimate of ADV head motion and removing that  
<sup>190</sup> motion from the measured signal. Previous works have utilized inertial motion sensors to quantify  
<sup>191</sup> the motion of multiscale profilers for the purpose of measuring the full spectrum of oceanic shear  
<sup>192</sup> (Winkel et al. 1996). Nortek's ADV-IMU measures the linear acceleration,  $\vec{a}$ , rotational motion,  
<sup>193</sup>  $\vec{\omega}$ , and orientation matrix,  $\mathbf{R}$ , of the ADV pressure case (body) in the Earth reference frame. So  
<sup>194</sup> long as the ADV head is rigidly connected to the ADV pressure case, it is possible to utilize the  
<sup>195</sup> IMU motion signals to calculate the motion of the ADV head and remove it from the measured  
<sup>196</sup> velocity signal. A similar approach has been used to correct sonic anemometer measurements of  
<sup>197</sup> atmospheric turbulence (e.g., Miller et al. 2008). The ADV head motion is calculated as the sum  
<sup>198</sup> of rotational and translational motion:

$$\begin{aligned} \vec{u}_h &= \vec{u}_{\omega} + \vec{u}_a + \vec{u}_{low} \\ &= \mathbf{R}^T \cdot \vec{\omega}^*(t) \times \vec{l}^* + \int \{\vec{a}(t)\}_{HP(f_a)} dt + \vec{u}_{low} \end{aligned} \quad (2)$$

199 Here,  $*$  superscripts denote quantities in the ADV's local coordinate system, and  $\vec{\ell}^*$  is the vec-  
200 tor from the IMU to the ADV head.  $\mathbf{R}^T$ —the inverse of the orientation matrix—rotates vectors  
201 from the IMU to the Earth reference frame. The notation  $\{\vec{a}\}_{HP(f_a)}$  indicates that the IMU's  
202 accelerometer signal is high-pass filtered (in the Earth's stationary reference frame) at a chosen  
203 filter-frequency,  $f_a$ . This is necessary because accelerometers have low-frequency noise, some-  
204 times referred to as bias-drift (Barshan and Durrant-Whyte 1995; Bevly 2004; Gulmammadov  
205 2009).

206 Integrating  $\vec{a}$  to estimate  $\vec{\tilde{u}}_a$  amplifies the bias-drift noise at low frequencies, which dramatically  
207 reduces the signal-to-noise ratio at those time scales (Figure A1). The high-pass filtering reduces  
208 this noise so that it does not contaminate motion correction, but real motion that exists at these  
209 frequencies is still lost in the low signal-to-noise ratio (Egeland 2014; VanZwieten et al. 2015).  
210 This means that low-frequency motion is not well resolved by the IMU, and so there is a residual  
211 low-frequency translational motion,  $\vec{\tilde{u}}_{\text{low}}$ , that needs to be measured independently—or at the very  
212 least considered—when using motion-corrected ADV-IMU data. The  $\vec{\omega}$  and  $\vec{\tilde{u}}_\omega$  estimates do not  
213 have the same issue because there is no integration involved, and because low-frequency bias-drift  
214 in the  $\vec{\omega}$  sensors is stabilized by the IMU's on-board Kalman filtering (i.e., the accelerometer and  
215 magnetometer signals provide estimates of down and north, respectively, which stabilize orienta-  
216 tion estimates and eliminates bias from rotation estimates).

217 The choice of a high-pass filter for reducing low-frequency accelerometer noise depends on the  
218 flow conditions of the measurement and the platform being used. In particular, filter selection in-  
219 volves a trade-off between filtering out the bias-drift noise while not filtering out measured motion  
220 that is unresolved by an independent measurement of  $\vec{\tilde{u}}_{\text{low}}$ . If an independent measure of low-  
frequency motion is available it can be used to increase the accuracy of  $\vec{\tilde{u}}_h$  at low frequency. Note

222 that, to avoid double counting,  $\vec{u}_{\text{low}}$  should be estimated by applying the complementary low-pass  
223 filter to the independent measurement of low-frequency motion.

224 With this estimate of ADV head motion, it is straightforward to correct the measured velocity,  
225  $\vec{u}_{\text{m}}$ , to estimate the velocity in the Earth's inertial reference frame:

$$\vec{u}(t) = \vec{u}_{\text{m}}(t) + \vec{u}_{\text{h}}(t). \quad (3)$$

226 Note here that the '+'-sign is correct because head motion,  $\vec{u}_{\text{h}}$ , induces a measured velocity in the  
227 opposite direction of the head motion itself ( $\vec{u}_{\text{m}} = \vec{u} - \vec{u}_{\text{h}}$ ).

228 For the TTM and turbulence torpedo, we utilize  $f_a = 0.0333\text{Hz}$  (30-s period) and assume that  
229  $\vec{u}_{\text{low}} = 0$ . For the StableMoor buoy,  $f_a = 0.2\text{Hz}$  (5-s period). The bottom-track velocity was low-  
230 pass filtered at this frequency to provide an estimate of  $\vec{u}_{\text{low}}$ , and  $\vec{a}$  was high-pass filtered at this  
231 frequency. We use 4-pole, bidirectional (zero-phase), Hanning filters for all filtering operations.

232 Additional details on motion correction—including a detailed accounting of the distinct co-  
233 ordinate systems of the IMU, ADV pressure case, and ADV head—can be found in Kilcher  
234 et al. (2016). Open-source Python tools for performing motion correction of ADV-IMU data—  
235 including scripts that write processed data in Matlab and tabulated formats—are available at  
236 <http://lkilcher.github.io/dolfin/>.

## 237 4. Results

### 238 a. Mean velocity

239 Figure 7 shows a comparison of  $\vec{u}$  measured by an ADV-IMU mounted on a TTM, to an upward-  
240 looking acoustic Doppler profiler mounted on the TTM anchor. This comparison shows excellent  
241 agreement between the ADV and Doppler profiler measurements of mean velocity. The  $\bar{u}$ ,  $\bar{v}$ , and  
242  $\bar{w}$  components have a root-mean-square error of 0.05, 0.13, and 0.03 m/s, respectively. Although

<sup>243</sup> it is important to note that there is some discrepancy between ADP- and ADV-measured velocities  
<sup>244</sup> (especially in  $\bar{v}$ , which is most likely due to incomplete motion correction), the agreement between  
<sup>245</sup> the magnitude and direction of these independent velocity measurements indicates that moored  
<sup>246</sup> ADV-IMUs provide a reliable estimate of velocity in the Earth's reference frame.

<sup>247</sup> *b. TTM spectra*

<sup>248</sup> As discussed in detail in Part 1, the mooring motion of the TTM,  $S\{\vec{u}_h\}$ , has a peak at 0.1 to 0.2  
<sup>249</sup> Hz from swaying of the mooring that is most likely driven by eddy shedding from the spherical  
<sup>250</sup> buoy (Figure 8, red lines). There is also higher-frequency broadband motion that is associated  
<sup>251</sup> with fluttering of the strongback fin around the mooring line. Both of these motions are especially  
<sup>252</sup> energetic in the  $v$ -component spectra because this is the direction in which the TTM mooring  
<sup>253</sup> system is most unstable. As is expected from fluid-structure interaction theory, the amplitude of  
<sup>254</sup> these motions increases with increasing mean velocity (Morison et al. 1950).

<sup>255</sup> The mooring motion contaminates the uncorrected ADV measurements of velocity,  $S\{\vec{u}_m\}$ ,  
<sup>256</sup> whenever the amplitude of the motion is similar to or greater than the amplitude of the turbulence.  
<sup>257</sup> Fortunately, much of this motion can be removed using the IMU's motion signals as detailed in  
<sup>258</sup> Section 3. Lacking an independent measurement of turbulence velocity at this site, we interpret  
<sup>259</sup> the agreement of these spectra with turbulence theory as evidence of the success of the method.  
<sup>260</sup> In particular, at high frequencies ( $f > 0.3$  Hz) for each mean-flow speed, the spectra decay with  
<sup>261</sup> a  $f^{-5/3}$  slope and have equal amplitude across the velocity components. These results are con-  
<sup>262</sup> sistent with Kolmogorov's (1941) theory of isotropic turbulence, and are consistent with spectral  
<sup>263</sup> shapes of earlier measurements of turbulence in energetic tidal channels from stationary platforms  
<sup>264</sup> (Walter et al. 2011; Thomson et al. 2012; McMillan et al. 2016).

265 For  $|\vec{u}| > 1.0$ , motion correction modifies the  $u$  and  $v$  component spectra at frequencies as high  
266 as 3 Hz. This outcome indicates that in order for motion correction to be effective, synchronization  
267 between the ADV and IMU needs to be within 1/3 s or better. This suggests that asynchronous  
268 approaches to motion correction may be challenging, especially considering that the clock drift of  
269 some instrumentation can be as high as a few seconds per day. By integrating the IMU data into  
270 the ADV data stream, the Nortek ADV-IMU achieves a synchronization to within 1e-2 s.

271 At low frequencies the spectra tend to become roughly constant (especially at higher flow  
272 speeds), which is also consistent with previous works. Note that the very low magnitude of  $S\{\vec{u}_h\}$   
273 at low frequencies is partially a result of filtering the IMU's accelerometer signal when calculating  
274  $\vec{u}_a$ . The true low-frequency spectrum of ADV head motion is unknown (indicated using a dashed  
275 line below  $f_a$ ). A comparison of  $S\{\vec{u}\}$  measured by the TTM to that measured by the ADP—during  
276 the June 2012 deployment—reveals agreement at low frequencies (not shown). This finding sug-  
277 gests that the assumption that  $\vec{u}_{low} = 0$  at these frequencies and at this site for this platform is  
278 justified—even if  $S\{\vec{u}_h\}$  is not as low as indicated in Figure 8.

279 As successful as motion correction is, some of the motion contamination persists in  $S\{\vec{u}\}$ . This  
280 is most notable in  $S\{v\}$  at the highest flow speeds ( $> 2.0$  m/s): a peak at 0.15 Hz is an order of  
281 magnitude larger than a spectral fit to the other frequencies would indicate. This persistent motion  
282 contamination is evident to a lesser degree in  $S\{u\}$  for  $|u| > 2$  m/s, and in  $S\{v\}$  at lower flow  
283 speeds.  $S\{w\}$  appears to have no persistent motion contamination because the amplitude of the  
284 motion in this direction is much lower than for the other two components. For these measurements,  
285  $S\{w_h\}$  is so low that  $w$ -component motion correction makes only a minor correction to the spectra.

286 The amplitude of the persistent motion contamination peaks in  $S\{v\}$  at 0.15 Hz is a factor of 5  
287 to 10 times smaller than the amplitude of the ADV head motion itself. This observation suggests  
288 that the Microstrain IMU can be used to effectively correct mooring motion at 0.15 Hz when

289 the amplitude of that motion is less than 5 times the amplitude of the real turbulence spectrum.

290 As a result, we have chosen a value of 3 as a conservative estimate of the motion correction's  
291 effectiveness.

292 In addition to the primary benefit of correcting for mooring motion, the IMU measurements  
293 can also be used to identify and screen out persistent motion contamination. For example, one  
294 of the most common uses of turbulence spectra is for the calculation of  $\varepsilon$  and tke. For these  
295 purposes, and based on the relative amplitudes of the 0.15-Hz peaks, we assume that persistent  
296 motion contamination is likely, where  $S\{\vec{u}_h\}/S\{\vec{u}\} > 3$ , and thereby exclude these regions from  
297 spectral fits.

298 In the present case, for the  $u$  and  $w$  spectra, this criteria only excludes a narrow range of frequen-  
299 cies at the 0.15-Hz motion peak for some cases. This criteria is more restrictive of the  $v$ -component  
300 spectra at high frequencies for  $\bar{U} > 1.0$  m/s, but this may be acceptable because the amplitude of  
301  $S\{v\}$  at these frequencies—i.e., in the isotropic inertial subrange—should be equal to that of  $S\{u\}$   
302 and  $S\{w\}$  (Kolmogorov 1941).

303 Agreement of the  $v$ -component spectral amplitude with that of  $u$  and  $w$  at frequencies  $> 0.3$  Hz  
304 indicates that motion correction is effective at those frequencies even when  $S\{\vec{u}_h\}/S\{\vec{u}\} \gtrsim 3$ . This  
305 outcome suggests that our screening threshold is excessively conservative at those frequencies,  
306 and that a more precise screening threshold may be frequency dependent. For example, it might  
307 take into account the  $f^3$  character of the noise in  $S\{\vec{u}_a\}$  (Figure A1). For the purpose of this work,  
308 the  $S\{\vec{u}_h\}/S\{\vec{u}\} < 3$  threshold for spectral fits is sufficient, and detailed characterization of the  
309 IMU's motion- and frequency-dependent noise level is left for future work.

310    *c. StableMoor Spectra*

311    The spectra of the StableMoor motion has a broader peak with a maximum amplitude that is ap-  
312    proximately half the frequency of the TTM spectral peak (Figure 9). The motion of this platform  
313    also does not have high-frequency “subpeaks” or other high-frequency broadband excitation  
314    (Part 1). These characteristics of the motion are most likely due to the more massive and hydro-  
315    dynamically streamlined properties of the platform.

316    Like the TTM, the motion-corrected spectra from the StableMoor buoy are consistent with turbu-  
317    lence theory and previous observations. Most importantly, there is an improvement in the quality  
318    of the motion-corrected spectra compared to the TTM. In particular, the persistent motion con-  
319    tamination peaks are completely removed. That is, this measurement system provides an accurate  
320    estimate of the turbulence spectra at this location from low frequencies to more than 1Hz—well  
321    into the inertial subrange—for all three components of velocity.

322    Note that this level of accuracy cannot be obtained without the independent estimate of  $\vec{u}_{\text{low}}$ .  
323    If we assume that  $\vec{u}_{\text{low}} = 0$ , a similar plot to Figure 9 (not shown) reveals persistent motion-  
324    contamination peaks and troughs in the  $u$  and  $v$  spectra regardless of the choice of  $f_a$ . This as-  
325    sumption indicates that the low-frequency motion of the StableMoor buoy is below a threshold in  
326    which the IMU’s signal-to-noise ratio is high enough to resolve its motion. In other words, com-  
327    pared to the TTM, the StableMoor platform provides a more accurate measurement of turbulence  
328    when it includes an independent measure of  $\vec{u}_{\text{low}}$  (here a bottom-tracking ADCP), but it does no  
329    better—and perhaps worse—when it does not.

330    *d. Torpedo spectra*

331    The  $u$  and  $v$  motion of the turbulence torpedo is broadband and the  $w$  motion has a narrow  
332    peak at 0.3 Hz (Figure 10). Because  $\vec{u}_h$  is estimated using  $f_a = 0.0333\text{Hz}$  and assuming  $\vec{u}_{\text{low}} = 0$ ,

its spectra rolls off quickly below  $f_a$ . Motion correction of the torpedo data appears to effectively remove a motion peak from  $S\{w\}$  at 0.3 Hz, and straightens out  $S\{v\}$  between 0.04 and 0.6 Hz.  $S\{u\}$  is mostly unaffected by motion at these frequencies, because the torpedo motion is smaller than the turbulence in this direction. At frequencies below  $f_a$ ,  $S\{u\}$  and  $S\{v\}$  increase dramatically. This increase suggests that unresolved, low-frequency motion of the torpedo is contaminating the velocity measurements at these frequencies. It may be possible to correct for some of this contamination using a measurement of the ship's motion as a proxy for the torpedo's low-frequency motion, but this has not been done. Still, above  $f_a$ , the torpedo appears to provide a reliable estimate of spectral amplitude in the inertial subrange and can therefore be used to estimate  $\varepsilon$ . Considering the simplicity of the platform, it may be a useful option for quantifying this essential turbulence quantity in a variety of scenarios. Further, if a GPS is positioned above it, it may be capable of providing even more.

#### 345 e. Cross Spectra

346 Inspection of cross spectra from TTM measurements demonstrates that motion correction can  
347 reduce motion contamination to produce reliable estimates of velocity cross spectra (Figure 11).  
348 At low flow speeds (left column), cross spectra between components of  $\vec{u}_h$  (i.e., between compo-

349 nents of head motion, red) are small compared to correlated velocities. As the velocity magnitude  
350 increases (center and right columns), the swaying motion of the TTM at 0.15 Hz appears as a peak  
351 in the amplitude of the cross spectra of  $\vec{u}_h$  (red) and  $\vec{u}_m$  (black) for all three components of cross  
352 spectra (rows). Fortunately, motion correction reduces the amplitude of this peak dramatically so  
353 that  $C\{\vec{u}\}$  (blue) is small at 0.15 Hz compared to lower frequencies. Furthermore, the fact that the  
354 standard deviation of  $C\{\vec{u}\}$  is also relatively small at 0.15 Hz suggests that motion correction is  
355 effective for each spectral window, not just in their mean.

356 These results indicate that motion-corrected TTM velocity measurements can be used to obtain  
357 reliable estimates of turbulence Reynold's stresses, which are the integral of the cross spectra.  
358 Without motion correction, Reynold's stress estimates would be contaminated by the large peaks  
359 in the cross spectra that are caused by the swaying and fluttering motion of the TTM vane.

360 A similar investigation of StableMoor cross spectra (not shown) indicates that cross-spectral  
361 motion contamination is at a much lower amplitude than for the TTM. The low-frequency (< 0.3  
362 Hz) "swimming" motion of that platform produces a minimal cross-spectral signal, and the relative  
363 large mass of the platform minimizes the kinds of higher-frequency swaying and fluttering that  
364 creates large values of cross-spectral head motion. Thus, the StableMoor platform also produces  
365 reliable estimates of Reynold's stresses, which are presumed to be improved by motion correction.

## 366 5. Discussion

367 The previous section presented a comparison of  $\vec{u}$  measured by a TTM-mounted ADV to mea-  
368 surements from a co-located ADP. This comparison demonstrated that the IMU provides a reliable  
369 estimate of the ADV's orientation and that this can be utilized to estimate mean velocity in the  
370 Earth's reference frame. Turbulence velocity estimates from the same ADP are also in agree-  
371 ment with low-frequency TTM turbulence estimates (not shown), but the ADP does not resolve  
372 turbulence at the scales where motion contamination is strongest (0.1 to 1.0 Hz).

373 Ideally, moored motion-corrected turbulence velocity measurements would be validated against  
374 simultaneous independent validated measurements of turbulence velocity at the same scales and  
375 exact time and location. Accomplishing this, however, involves significant technical challenges  
376 that are not easily overcome—most notably the difficulty of measuring turbulence at the same point  
377 as the moving ADV. A slightly less ideal but much more realistic confirmation of the methodology  
378 might involve comparing the statistics of moored turbulence measurements to those from a nearby

fixed platform, or a fixed platform placed at the same location at a different time (e.g., the “TTT” platform described in Thomson et al. 2012). Unfortunately, to our knowledge, these measurements have not yet been made.

Lacking a relevant, fixed, independent turbulence measurement to compare to it is instructive to demonstrate the degree to which the moored measurements are consistent with turbulence theory and other turbulence measurements in similar flow environments. The previous section showed that the shape of the turbulence velocity spectra from moored ADVs is consistent with Kolmogorov’s theory of locally isotropic turbulence, which has been observed consistently in turbulence measurements for decades (Kolmogorov 1941; Grant et al. 1962; McMillan et al. 2016). In particular, we observed an isotropic subrange—an  $f^{-5/3}$  spectral slope and equal amplitude spectra between components—that is driven by anisotropic turbulence at longer timescales (Figures 8, 9, 10). This finding is interpreted as the first indication that the measurement systems presented are capable of accurately resolving turbulence. The degree to which uncorrected spectra were corrected toward this theoretical and observationally confirmed shape is interpreted as a measure of the improvement of the spectral estimates by motion correction.

Figure 12 presents a time series of the mean velocity (A) and several turbulence statistics that were measured during the June 2014 TTM deployment. This figure shows the evolution of the flow through Admiralty Inlet during 1.5 tidal cycles. The tke (B), Reynold’s stresses (C), dissipation, and one component of turbulence production (D) grow and strengthen with ebb or flood then subside during slack tide. This component of turbulence production is:

$$P_{uz} = \frac{\partial \bar{u}}{\partial z} \bar{u} w . \quad (4)$$

Where  $\partial \bar{u} / \partial z$  is computed from the two ADVs on the TTM. The highest values of  $\varepsilon$  and  $P_{uz}$  occur at the peak of the ebb or flood, which is in agreement with other measurements in tidal channels.

401 The agreement of the magnitude of  $P_{uz}$  with  $\varepsilon$  at those times suggests a local production-dissipation  
402 balance that is often observed in tidally forced channels (Trowbridge et al. 1999; Stacey et al.  
403 1999b; McMillan et al. 2016). At other times, the value of  $P_{uz}$  is insufficient to balance  $\varepsilon$  or is  
404 negative.

405 Inspection of the negative  $P_{uz}$  values reveals that most of them are caused by a reversed sign of  $\bar{uw}$   
406 rather than a reversed sign of  $\partial u / \partial z$  (i.e., when compared to the sign of  $u$ ). This finding suggests  
407 that uncertainty in  $\bar{uw}$  may be contributing to discrepancies between  $P_{uz}$  and  $\varepsilon$ . Furthermore,  
408 considering the complex nature of the shoreline near this site (i.e., the headland), it is not surprising  
409 that  $P_{uz}$  does not balance  $\varepsilon$  perfectly. Other terms of the the equation are likely to be important,  
410 such as other components of production, advection terms, or turbulent transport terms. The fact  
411 that these two terms are in near balance as often as they are is a strong indication that bottom  
412 boundary layer physics are important to the dynamics at this site.

413 Figure 13 compares individual values of  $P_{uz}$  with  $\varepsilon$  directly. Given the assumptions implicit in  
414 this comparison and the discussion above, the agreement between  $P_{uz}$  and  $\varepsilon$  is an encouraging  
415 result that suggests the turbulent boundary reaches the depth of these measurements (10 m) during  
416 the highest flow speeds. This result is further supported by a comparison of  $\bar{U}$  with  $\varepsilon$  (Figure  
417 14). Here we see a  $\varepsilon \propto \bar{U}^3$  dependence that is again suggestive of bottom boundary layer physics  
418 (Trowbridge 1992; Nash et al. 2009). At lower flow speeds,  $\varepsilon$  deviates from this relationship,  
419 which suggests that the boundary layer is no longer the dominant physical process at the depth of  
420 these measurements.

## 421 6. Conclusion

422 This work presents a methodology for measuring turbulence from moored ADV-IMUs and de-  
423 tails an approach for removing the IMU-measured mooring motion from the ADV's velocity mea-

424    surements. The IMU integrated into the Nortek Vector ADV has been configured to provide esti-  
425    mates of the ADV’s orientation and motion at every time step of the ADV’s sampling. The tight  
426    integration of the IMU and ADV data streams provides a data set that can be used to correct ve-  
427    locity measurements for mooring motion and rotate those measurements into the Earth’s reference  
428    frame.

429    Comparison of spectra of ADV head motion,  $S\{\vec{u}_h\}$ , to that of motion-corrected,  $S\{\vec{u}\}$ , and  
430    uncorrected spectra,  $S\{\vec{u}_m\}$ , reveals that motion correction improves spectral estimates of moored  
431    ADV measurements. In particular, we found that motion-corrected spectra have spectral shapes  
432    that are similar to previous measurements of tidal-channel turbulence and have a  $f^{-5/3}$  spectral  
433    slope at high frequencies. This finding suggests that the motion-corrected spectra resolve the  
434    inertial subrange predicted by Kolmogorov’s theory of locally isotropic turbulence.

435    Motion correction reduces motion contamination for all platforms we presented but it does not  
436    necessarily remove it completely. This outcome seems to depend on the relative amplitude of  
437    platform motion compared to the underlying turbulence being measured. The most notable ex-  
438    ample of this is from the TTM, which has a large “swaying” peak at 0.1 Hz. Where this peak  
439    is very large—especially in the  $v$  component—it is not reduced to a level that is consistent with  
440    earlier measurements of tidal-channel turbulence—i.e., there is no smooth roll-off between the  
441    low-frequency energy-containing scales and the  $f^{-5/3}$  inertial subrange.

442    This inconsistency indicates that turbulence measurements from moored, motion-corrected IMU  
443    ADVs must be interpreted with care. An inspection of spectra presented here suggests that exclud-  
444    ing spectral regions where  $S\{\vec{u}_h\}/S\{\vec{u}\} > 3$  removes persistent-motion contamination peaks while  
445    still preserving spectral regions where motion correction is effective. Using this criteria, it is then  
446    possible to produce spectral fits that exclude persistent-motion contamination, and provide reliable  
447    estimates of turbulence quantities of interest (e.g.,  $\varepsilon$  and tke).

448 We've also shown that motion correction reduces motion contamination in cross spectra. This  
449 finding is important because it suggests that moored IMU-ADV measurements may be used to  
450 produce reliable estimates of Reynolds stresses. We utilized these stress estimates and vertical  
451 shear estimates, both from the TTM, to estimate  $P_{uz}$ .

452 Finally, we have shown that  $\varepsilon$  estimates based on motion-corrected spectra scale with the  $U^3$ , and  
453 balance  $P_{uz}$  estimates during ebb and flood. Together, these results indicate that bottom boundary  
454 layer physics are a dominant process at this site, and that the boundary layer reaches the height  
455 of the IMU ADVs (10 m) during ebb and flood. The degree of agreement between  $P_{uz}$  and  $\varepsilon$  also  
456 serves as an indicator of the self-consistency of moored IMU-ADV turbulence measurements.

457 *Acknowledgments.* Many thanks to Joe Talbert, Alex DeKlerk, Captain Andy Reay-Ellers, Jen-  
458 nifer Rinker, Maricarmen Guerra, and Eric Nelson in assisting with data collection. The authors  
459 are also grateful to James VanZwieten, Matthew Egeland and Marshall Richmond for discussion  
460 on the details of this work.

461 This work was supported by the U.S. Department of Energy under Contract No. DE-AC36-  
462 08GO28308 with the National Renewable Energy Laboratory. Funding for the work was provided  
463 by the DOE Office of Energy Efficiency and Renewable Energy, Wind and Water Power Technolo-  
464 gies Office.

465 The U.S. Government retains and the publisher, by accepting the article for publication, ac-  
466 knowledges that the U.S. Government retains a nonexclusive, paid-up, irrevocable, worldwide  
467 license to publish or reproduce the published form of this work, or allow others to do so, for U.S.  
468 Government purposes.

## APPENDIX

470 A1. Comparing StableMoor  $\vec{u}_{\text{low}}$  to IMU  $\vec{u}_{\text{h}}$ 

471 To better understand the IMU's signal-to-noise ratio, we compare the motion of the StableMoor  
 472 buoy from the ADP bottom track measurements,  $\vec{u}_{\text{BT}}$ , to the IMU's estimates of ADP motion.

473 To do this, we compute the IMU's estimate of ADP motion using equation (2), and replacing  $\ell^*$   
 474 with the vector that points from the IMU to the ADP head. We then linearly interpolate the ADP  
 475 measurements of  $\vec{u}_{\text{BT}}$  onto the times of the ADV-IMU measurements.

476 The coherence between these two signals is high and statistically significant over 1.5 decades—  
 477 from 0.03 to 0.8 Hz (Priestley 1981). The  $v$  component has the highest coherence, 98%, because  
 478 this is the direction that has the most motion (i.e., these estimates have a higher signal-to-noise  
 479 ratio). The  $u$  and  $w$  components have a slightly lower coherence, 80% and 65%, respectively.

480 On the low-frequency side, our interpretation is that the signal-to-noise ratio of the IMU in-  
 481 creases dramatically below 0.03 Hz, resulting in low coherence. On the high-frequency side,  
 482 Doppler noise in the ADP measurements contaminates its estimates of motion, causing the de-  
 483 crease in coherence at 0.8 Hz. A comparison of the phase between these signals shows that there  
 484 is no lag between the measurements (not shown).

485 These results help to inform the selection of zero-lag filters used to estimate  $\vec{u}_{\text{low}}$  from  $\vec{u}_{\text{BT}}$ .  
 486 In particular, by selecting 0.2 Hz, we target the middle of the coherence peak between the two  
 487 measurements. Furthermore, the rapid decrease in coherence below 0.03 Hz provides an objective  
 488 measurement of the frequency at which IMU measured velocity becomes unreliable in the flow  
 489 conditions we observed.

490    **References**

- 491    Afgan, I., J. McNaughton, S. Rolfo, D. Apsley, T. Stallard, and P. Stansby, 2013: Turbulent flow  
492    and loading on a tidal stream turbine by les and rans. *International Journal of Heat and Fluid*  
493    *Flow*, **43**, 96–108.
- 494    Alexander, S. R., and P. E. Hamlington, 2015: Analysis of turbulent bending moments in tidal  
495    current boundary layers. *Journal of Renewable and Sustainable Energy*, **7 (6)**, 063 118.
- 496    Alford, M. H., 2010: Sustained, full-water-column observations of internal waves and mixing near  
497    mendocino escarpment. *Journal of Physical Oceanography*, **40 (12)**, 2643–2660, doi:10.1175/  
498    2010JPO4502.1.
- 499    Bachmann, E. R., X. Yun, D. McKinney, R. B. McGhee, and M. J. Zyda, 2003: Design and imple-  
500    mentation of MARG sensors for 3-DOF orientation measurement of rigid bodies. *International*  
501    *Conference on Robotics & Automation*, Taipei, Taiwan.
- 502    Barshan, B., and H. F. Durrant-Whyte, 1995: Inertial navigation systems for mobile robots. *IEEE*  
503    *Transactions on Robotics and Automation*, **11 (3)**, 328–342.
- 504    Bevly, D. M., 2004: Global positioning system (gps): A low-cost velocity sensor for correcting in-  
505    erial sensor errors on ground vehicles. *Journal of dynamic systems, measurement, and control*,  
506    **126 (2)**, 255–264.
- 507    Cartwright, G. M., C. T. Friedrichs, P. J. Dickhudt, T. Gass, and F. H. Farmer, 2009: Using the  
508    acoustic doppler velocimeter (adv) in the mudbed real-time observing system. *Marine Technol-*  
509    *ogy for Our Future: Global and Local Challenges*.
- 510    Doherty, K., D. Frye, S. Liberatore, and J. Toole, 1999: A moored profiling instrument\*. *Journal*  
511    *of Atmospheric and Oceanic Technology*, **16 (11)**, 1816–1829.

- 512 Egeland, M. N., 2014: Spectral evaluation of motion compensated ADV systems for ocean turbu-  
513 lence measurements. Ph.D. thesis, Florida Atlantic University.
- 514 Fer, I., and M. B. Paskyabi, 2014: Autonomous ocean turbulence measurements using shear probes  
515 on a moored instrument. *Journal of Atmospheric and Oceanic Technology*, **31** (2), 474–490, doi:  
516 10.1175/JTECH-D-13-00096.1.
- 517 Finlayson, D., 2005: Combined bathymetry and topography of the Puget Lowlands, Washington  
518 state. URL <http://www.ocean.washington.edu/data/pugetsound/>.
- 519 Geyer, R. W., M. E. Scully, and D. K. Ralston, 2008: Quantifying vertical mixing in estuaries.  
520 *Environmental Fluid Mechanics*, **8**, 495–509, doi:10.1007/s10652-008-9107-2.
- 521 Goodman, L., E. R. Levine, and R. G. Lueck, 2006: On measuring the terms of the turbulent  
522 kinetic energy budget from an auv. *Journal of Atmospheric and Oceanic Technology*, **23** (7),  
523 977–990, doi:10.1175/JTECH1889.1.
- 524 Grant, H. L., R. W. Stewart, and A. Moilliet, 1962: Turbulence spectra from a tidal channel.  
525 *Journal of Fluid Mechanics*, **12**, 241–263.
- 526 Gulmammadov, F., 2009: Analysis, modeling and compensation of bias drift in mems inertial  
527 sensors. *Recent Advances in Space Technologies, 2009. RAST'09. 4th International Conference*  
528 *on*, IEEE, 591–596.
- 529 Gunawan, B., V. S. Neary, and J. Colby, 2014: Tidal energy site resource assessment in the East  
530 River tidal strait, near Roosevelt Island, New York, NY (USA). *Renewable Energy*, **71**, 509–  
531 517, doi:10.1016/j.renene.2014.06.002.

- 532 Hand, M. M., N. D. Kelley, and M. J. Balas, 2003: Identification of wind turbine response to  
533 turbulent inflow structures. Tech. Rep. NREL/CP-500-33465, National Renewable Energy Lab-  
534 oratory.
- 535 Harding, S., L. Kilcher, and J. Thomson, 2017: Turbulence measurements from compliant moor-  
536 ings - part 1: Motion characterization, in review.
- 537 Kelley, N. D., B. J. Jonkman, G. N. Scott, J. T. Bialasiewicz, and L. S. Redmond, 2005: The impact  
538 of coherent turbulence on wind turbine aeroelastic response and its simulation. *WindPower*,  
539 Denver, Colorado, NREL/CP-500-38074, may 15-18.
- 540 Kilcher, L., J. Thomson, J. Talbert, and A. DeKlerk, 2016: Measuring turbulence from moored  
541 acoustic Doppler velocimeters: A manual to quantifying inflow at tidal energy sites. 9 62979,  
542 National Renewable Energy Laboratory. URL [www.nrel.gov/docs/fy16osti/62979.pdf](http://www.nrel.gov/docs/fy16osti/62979.pdf).
- 543 Kim, S. C., C. T. Friedrichs, J. P.-Y. Maa, and L. D. Wright, 2000: Estimating bottom stress in  
544 tidal boundary layer from acoustic doppler velocimeter data. *Journal of Hydraulic Engineering*,  
545 399–406.
- 546 Kolmogorov, A. N., 1941: Dissipation of energy in the locally isotropic turbulence. *Dokl. Akad.*  
547 *Nauk SSSR*, **32** (1), 16–18, URL <http://www.jstor.org/stable/51981>.
- 548 Kraus, C., A. Lohrmann, and R. Cabrera, 1994: A new acoustic meter for measuring 3d laboratory  
549 flows. *Journal of Hydraulic Engineering*, **120**, 406–412.
- 550 Lohrmann, A., R. Cabrera, G. Gelfenbaum, and J. Haines, 1995: Direct measurements of reynolds  
551 stress with an acoustic doppler velocimeter. *Current Measurement, 1995.*, *Proceedings of the*  
552 *IEEE Fifth Working Conference on*, 205–210, doi:10.1109/CCM.1995.516175.

- 553 Lorke, A., 2007: Boundary mixing in the thermocline of a large lake. *Journal of Geophysical*  
554 *Research: Oceans*, **112 (C9)**, n/a–n/a, doi:10.1029/2006JC004008, c09019.
- 555 Lueck, R. G., and D. Huang, 1999: Dissipation measurement with a moored instrument in a swift  
556 tidal channel. *Journal of atmospheric and oceanic technology*, **16**, 1499–1505.
- 557 Lumley, J., and E. Terray, 1983: Kinematics of turbulence convected by a random wave field.  
558 *Journal of Physical Oceanography*, **13 (11)**, 2000–2007.
- 559 Marins, J. L., X. Yun, E. R. Bachmann, R. B. McGhee, and M. J. Zyda, 2001: An extended Kalman  
560 filter for quaternion-based orientation estimation using MARG sensors. *Internation cconference*  
561 *on intelligent robots and systems*.
- 562 McCaffrey, K., B. Fox-Kemper, P. E. Hamlington, and J. Thomson, 2015: Characterization of  
563 turbulence anisotropy, coherence, and intermittency at a prospective tidal energy site: Observa-  
564 tional data analysis. *Renewable Energy*, **76**, 441–453.
- 565 McMillan, J. M., A. E. Hay, R. G. Lueck, and F. Wolk, 2016: Rates of dissipation of turbulent  
566 kinetic energy in a high reynolds number tidal channel. *Journal of Atmospheric and Oceanic*  
567 *Technology*, **33 (4)**, 817–837, doi:10.1175/JTECH-D-15-0167.1.
- 568 MicroStrain, I., 2010: Technical note: Coning and sculling. Tech. Rep. I0019, MicroStrain. URL  
569 [http://files.microstrain.com/TN-I0019\\_3DM-GX3-25\\_\\_Coning\\_And\\_Sculling.pdf](http://files.microstrain.com/TN-I0019_3DM-GX3-25__Coning_And_Sculling.pdf).
- 570 MicroStrain, I., 2012: *3DM-GX3-15,-25 MIP Data Communications Protocol*. URL <http://files.microstrain.com/3DM-GX3-15-25-MIP-Data-Communications-Protocol.pdf>, retrieved  
571 January 2014.

- 573 Miller, S. D., T. S. Hristov, J. B. Edson, and C. A. Friehe, 2008: Platform motion effects on  
574 measurements of turbulence and air-sea exchange over the open ocean. *Journal of Atmospheric*  
575 and *Oceanic Technology*, **25** (9), 1683–1694, doi:10.1175/2008JTECHO547.1.
- 576 Morison, J. R., J. W. Johnson, and S. A. Schaaf, 1950: The force exerted by surface waves on  
577 piles. *Journal of Petroleum Technology*, **2** (05), 149–154.
- 578 Moum, J., and J. Nash, 2009: Mixing measurements on an equatorial ocean mooring. *Journal of*  
579 *Atmospheric and Oceanic Technology*, **26** (2), 317–336.
- 580 Mücke, T., D. Kleinhans, and J. Peinke, 2011: Atmospheric turbulence and its influence on the  
581 alternating loads on wind turbines. *Wind Energy*, **14**, 301–316.
- 582 Nash, J. D., L. F. Kilcher, and J. N. Moum, 2009: Structure and composition of a strongly  
583 stratified, tidally pulsed river plume. *Journal of Geophysical Research*, **114**, C00B12, doi:  
584 10.1029/2008JC005036.
- 585 Nash, J. D., E. Kunze, J. M. Toole, and R. W. Schmitt, 2004: Internal tide reflection and turbulent  
586 mixing on the continental slope. *Journal of Physical Oceanography*, **34** (5), 1117–1134, doi:  
587 10.1175/1520-0485(2004)034<1117:ITRATM>2.0.CO;2.
- 588 Nortek, 2005: *Vector Current Meter User Manual*. Vangkroken 2, NO-1351 RUD, Norway, h ed.
- 589 Paskyabi, M. B., and I. Fer, 2013: Turbulence measurements in shallow water from a subsurface  
590 moored moving platform. *Energy Procedia*, **35**, 307 – 316, doi:10.1016/j.egypro.2013.07.183.
- 591 Polagye, B., and J. Thomson, 2013: Tidal energy resource characterization: methodology and field  
592 study in admiralty inlet, Puget Sound, WA (USA). *Proceedings of the Institution of Mechanical*  
593 *Engineers, Part A: Journal of Power and Energy*, **227** (3), 352–367.

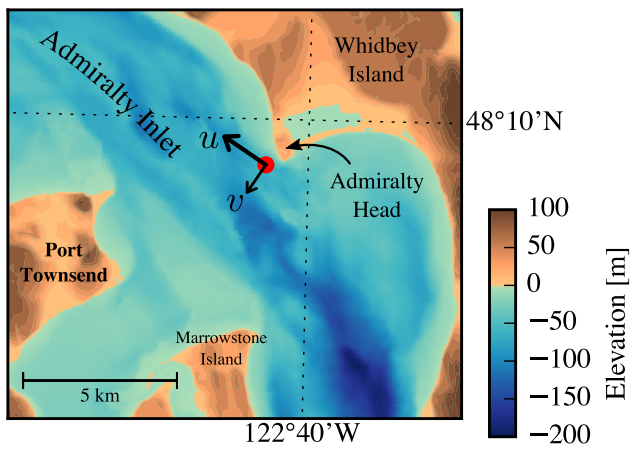
- 594 Priestley, M., 1981: *Spectral Analysis and Time Series*. Academic Press, London.
- 595 Rippeth, T. P., E. Williams, and J. H. Simpson, 2002: Reynolds stress and turbulent en-  
596 ergy production in a tidal channel. *Journal of Physical Oceanography*, **32**, 1242–1251, doi:  
597 10.1175/1520-0485(2002)032\$1242:RSATEP\$2.0.CO;2.
- 598 Sreenivasan, K. R., 1995: On the universality of the Kolmogorov constant. *Physics of Fluids*, **7**,  
599 2778–2784.
- 600 Stacey, M. T., S. G. Monismith, and J. R. Burau, 1999a: Measurements of reynolds stress  
601 profiles in unstratified tidal flow. *J. Geophys. Res.*, **104 (C5)**, 10 933–10 949, doi:10.1029/  
602 1998JC900095.
- 603 Stacey, M. T., S. G. Monismith, and J. R. Burau, 1999b: Observations of turbulence in a partially  
604 stratified estuary. *Journal of Physical Oceanography*, **29**, 1950–1970.
- 605 Thomson, J., B. Polagye, V. Durgesh, and M. Richmond, 2012: Measurements of turbulence at  
606 two tidal energy sites in Puget Sound, WA. *Journal of Oceanic Engineering*, **37 (3)**, 363–374,  
607 doi:10.1109/JOE.2012.2191656.
- 608 Trowbridge, J. H., 1992: A simple description of the deepening and structure of a stably stratified  
609 flow driven by a surface stress. *Journal of Geophysical Research*, **97**, 15 529–15 543.
- 610 Trowbridge, J. H., W. R. Geyer, M. M. Bowen, and A. J. I. Williams, 1999: Near-bottom turbu-  
611 lence measurements in a partially mixed estuary: turbulent energy balance, velocity structure  
612 and along-channel momentum balance. *Journal of Physical Oceanography*, **29**, 3056–3072.
- 613 van der Walt, S., S. C. Colbert, and G. Varoquaux, 2011: The numpy array: A structure for efficient  
614 numerical computation. *Computing in Science & Engineering*, **13**, 22–30, doi:10.1109/MCSE.  
615 2011.37.

- 616 VanZwieten, J. H., M. N. Egeland, K. D. von Ellenrieder, J. W. Lovenbury, and L. Kilcher, 2015:  
617 Experimental evaluation of motion compensated adv measurements for in-stream hydrokinetic  
618 applications. *Current, Waves and Turbulence Measurement (CWTM), 2015 IEEE/OES Eleventh,*  
619 1–8, doi:10.1109/CWTM.2015.7098119.
- 620 Voulgaris, G., and J. H. Trowbridge, 1998: Evaluation of the acoustic doppler velocimeter (adv)  
621 for turbulence measurements. *Journal of Atmospheric and Oceanic technology*, **15**, 272–289.
- 622 Walter, R. K., N. J. Nidzieko, and S. G. Monismith, 2011: Similarity scaling of turbulence spectra  
623 and cospectra in a shallow tidal flow. *Journal of Geophysical Research: Oceans*, **116 (C10)**.
- 624 Wiles, P. J., T. P. Rippeth, J. H. Simpson, and P. J. Hendricks, 2006: A novel technique for  
625 measuring the rate of turbulent dissipation in the marine environment. *Geophysical Research  
626 Letters*, **33**, 21 608.
- 627 Winkel, D., M. Gregg, and T. Sanford, 1996: Resolving oceanic shear and velocity with the multi-  
628 scale profiler. *Journal of Atmospheric and Oceanic Technology*, **13 (5)**, 1046–1072.
- 629 Wyngaard, J. C., L. Rockwell, and C. A. Friehe, 1985: Errors in the measurement of turbulence  
630 upstream of an axisymmetric body. *Journal of Atmospheric and Oceanic Technology*, **2 (4)**,  
631 605–614.
- 632 Zhang, Y., K. Streitlien, J. G. Bellingham, and A. B. Baggeroer, 2001: Acoustic doppler ve-  
633 locimeter flow measurement from an autonomous underwater vehicle with applications to deep  
634 ocean convection. *Journal of Atmospheric and Oceanic Technology*, **18 (12)**, 2038–2051, doi:  
635 10.1175/1520-0426(2001)018<2038:ADVFMF>2.0.CO;2.

## 636 LIST OF FIGURES

637	<b>Fig. 1.</b>	Bathymetry of Admiralty Inlet near Port Townsend, Washington, U.S.A. (Finlayson 2005). The red dot indicates the location of all measurements. The positive $u$ direction is the direction of ebb flow (thick arrow originating from red dot), and positive $v$ is away from Admiralty Head (smaller arrow).	33
641	<b>Fig. 2.</b>	Schematic diagram of the TTM; not to scale.	34
642	<b>Fig. 3.</b>	TTM components on the deck of the R/V Jack Robertson. The TTM includes two ADVs, with pressure cases mounted on opposite sides of the fin. The anchor stack includes a pop-up buoy for retrieval. The green arrow indicates the vector from the IMU to the ADV head (face of the transmit transducer).	35
646	<b>Fig. 4.</b>	Top: Alex DeKlerk checks to ensure that the StableMoor buoy is properly fastened to its anchor; the RDI workhorse ADCP can be seen in the rear instrument bay. A bridle is draped across the top of the buoy for deployment and recovery, and a small marker buoy fastened to the tail is useful during recovery. Bottom: a close-up of the StableMoor with the ADV head and the top of its pressure case. The green arrow indicates the vector from the IMU to the ADV head.	36
652	<b>Fig. 5.</b>	The turbulence platform showing details of the ADV head and pressure case configuration. The green arrow indicates the vector from the IMU to the ADV head. The head cable was taped out of the way beneath the sounding weight tail fins shortly after taking this photo.	37
655	<b>Fig. 6.</b>	Spectra of $\vec{u}_\omega$ (yellow) and $\vec{u}_a$ signals from the Microstrain IMU sitting on a motionless table. The $\vec{u}_a$ signals are unfiltered (black), and high-pass filtered at 30 s (magenta), 10 s (blue), 5 s (green). Vertical dotted lines indicate the filter frequency. The black horizontal dotted line indicates the noise level of a Nortek Vector ADV configured to measure $\pm 4 \text{ m/s}$ . The shaded region indicates the range of spectra presented herein ( $0.002 < \text{tke} < 0.03 \text{ m}^2/\text{s}^2$ , $1\text{e}-5 < \varepsilon < 5\text{e}-4 \text{ W/kg}$ ).	38
661	<b>Fig. 7.</b>	Time series of tidal velocity at Admiralty Head from TTM measurements (black), and an acoustic Doppler profiler (red). The profiler measurements—taken at the same depth as the ADV on the TTM—were contaminated by acoustic reflection from the strongback fin when it was inline with one of the profiler’s beams. Note that the vertical scale on the three axes vary by more than an order of magnitude; the small ticks in A and B are equivalent to the ticks in C.	39
667	<b>Fig. 8.</b>	Turbulence spectra from the June 2014 TTM deployment. Each column is for a range of streamwise velocity magnitudes (indicated at top). The rows are for each component of velocity (indicated to the lower right of the right column). The uncorrected spectra are in black and the corrected spectra are blue, and the spectra of ADV head motion, $\vec{u}_h$ , is red (also indicated in the legend). The vertical red dotted line indicates the filter frequency applied to the IMU accelerometers when estimating $\vec{u}_h$ ; below this frequency $S\{\vec{u}_h\}$ is plotted as a dashed line. Diagonal black dotted lines indicate a $f^{-5/3}$ slope. The number of spectral ensembles, $N$ , in each column is indicated in the top row.	40
675	<b>Fig. 9.</b>	Turbulence spectra from the StableMoor buoy. The axes layout and annotations are identical to Figure 8, except that $S\{\vec{u}_h\}$ is plotted as a solid line at all frequencies because it is measured at all frequencies.	41





706 FIG. 1. Bathymetry of Admiralty Inlet near Port Townsend, Washington, U.S.A. (Finlayson 2005). The red  
 707 dot indicates the location of all measurements. The positive  $u$  direction is the direction of ebb flow (thick arrow  
 708 originating from red dot), and positive  $v$  is away from Admiralty Head (smaller arrow).

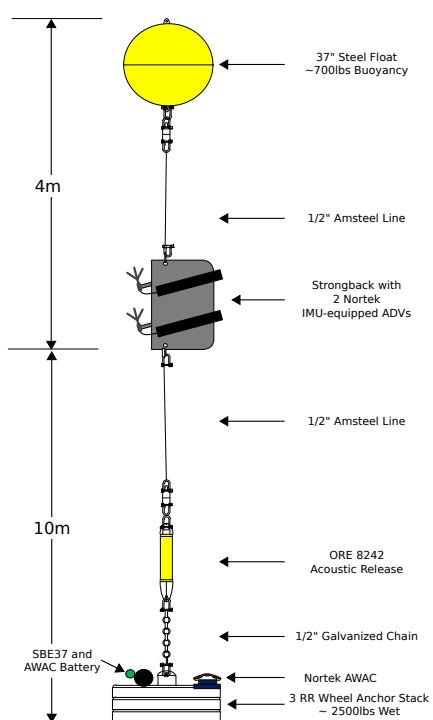


FIG. 2. Schematic diagram of the TTM; not to scale.



709 FIG. 3. TTM components on the deck of the R/V Jack Robertson. The TTM includes two ADVs, with  
710 pressure cases mounted on opposite sides of the fin. The anchor stack includes a pop-up buoy for retrieval. The  
711 green arrow indicates the vector from the IMU to the ADV head (face of the transmit transducer).



712 FIG. 4. Top: Alex DeKlerk checks to ensure that the StableMoor buoy is properly fastened to its anchor; the  
 713 RDI workhorse ADCP can be seen in the rear instrument bay. A bridle is draped across the top of the buoy  
 714 for deployment and recovery, and a small marker buoy fastened to the tail is useful during recovery. Bottom: a  
 715 close-up of the StableMoor with the ADV head and the top of its pressure case. The green arrow indicates the  
 716 vector from the IMU to the ADV head.



717 FIG. 5. The turbulence platform showing details of the ADV head and pressure case configuration. The green  
718 arrow indicates the vector from the IMU to the ADV head. The head cable was taped out of the way beneath the  
719 sounding weight tail fins shortly after taking this photo.

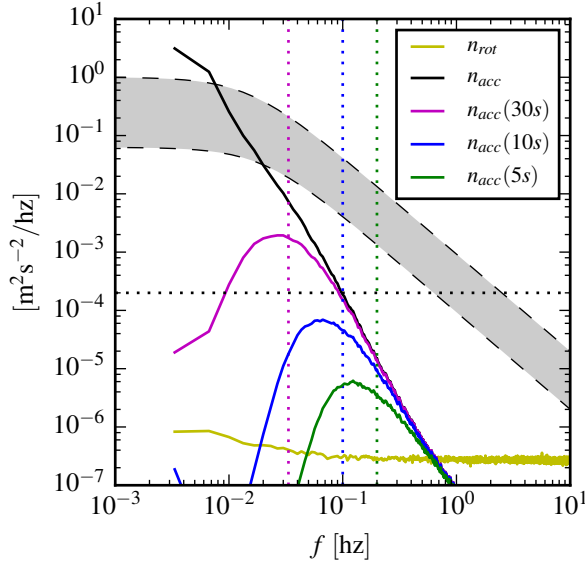


FIG. 6. Spectra of  $\vec{u}_\omega$  (yellow) and  $\vec{u}_a$  signals from the Microstrain IMU sitting on a motionless table. The  $\vec{u}_a$  signals are unfiltered (black), and high-pass filtered at 30 s (magenta), 10 s (blue), 5 s (green). Vertical dotted lines indicate the filter frequency. The black horizontal dotted line indicates the noise level of a Nortek Vector ADV configured to measure  $\pm 4 \text{ m/s}$ . The shaded region indicates the range of spectra presented herein ( $0.002 < \text{tke} < 0.03 \text{ m}^2/\text{s}^2$ ,  $1\text{e}-5 < \epsilon < 5\text{e}-4 \text{ W/kg}$ ).

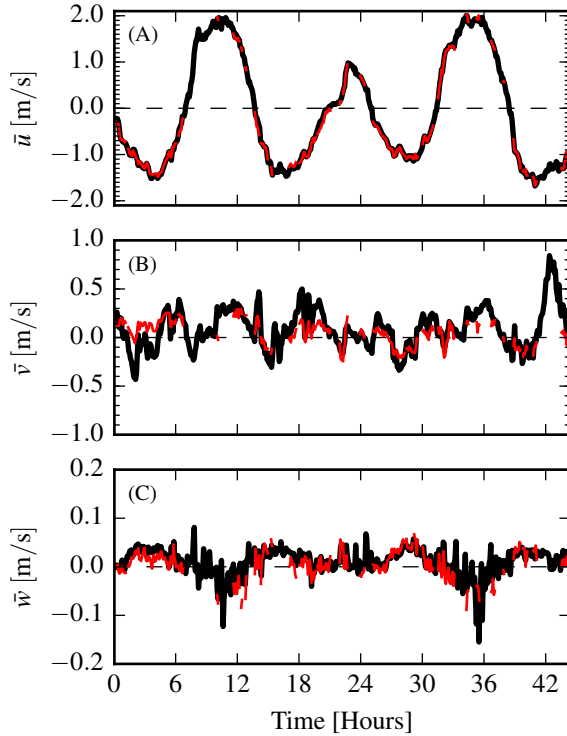
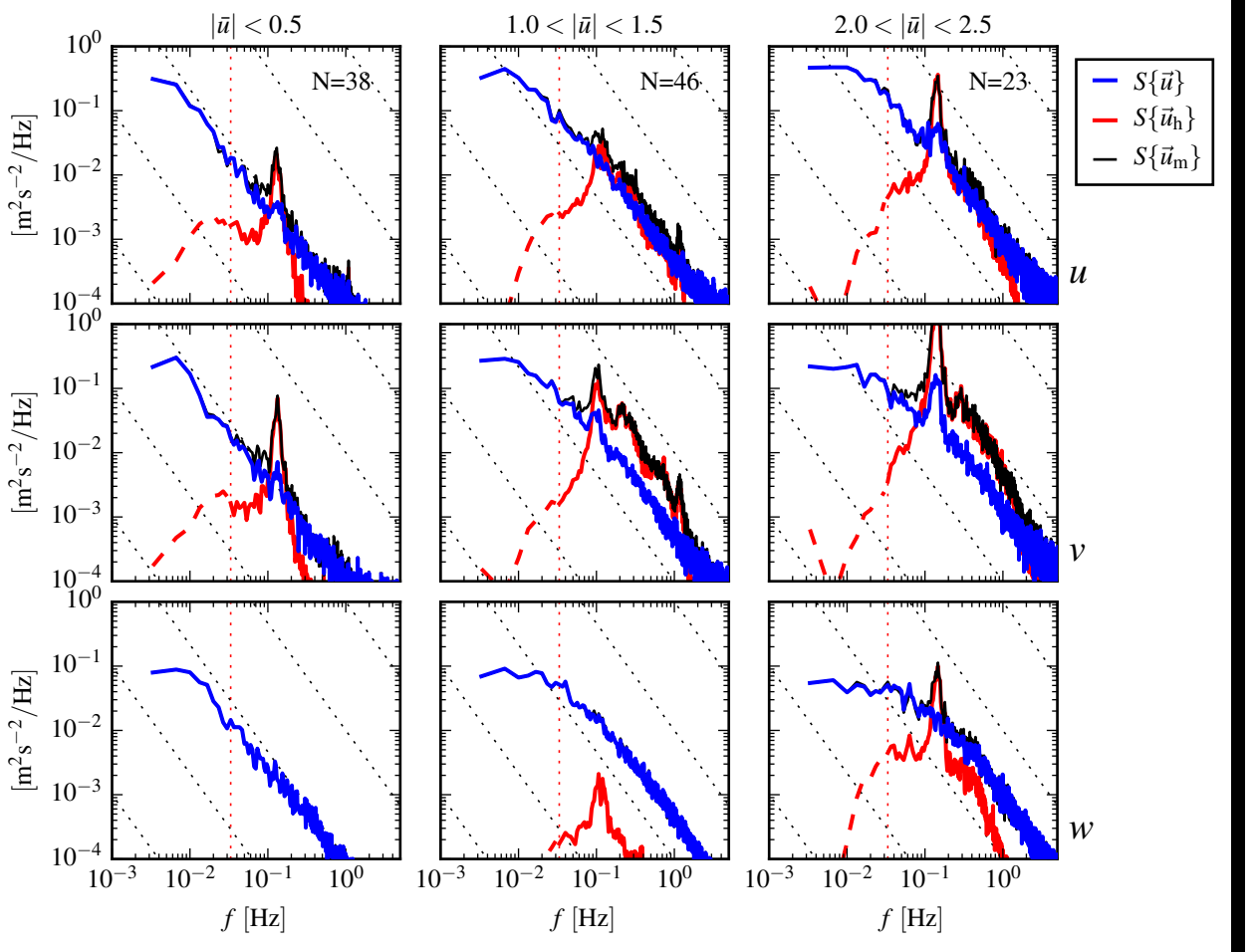
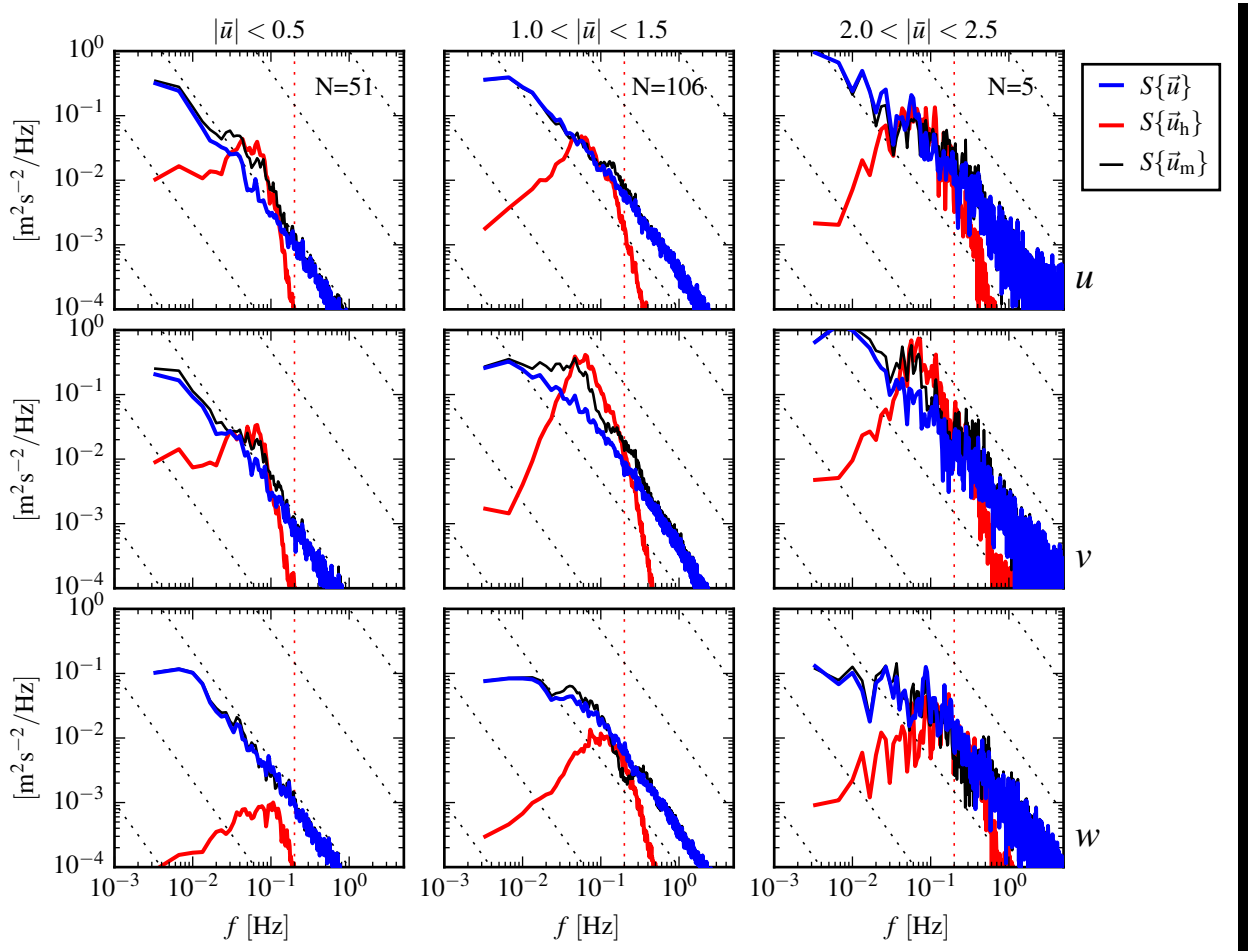


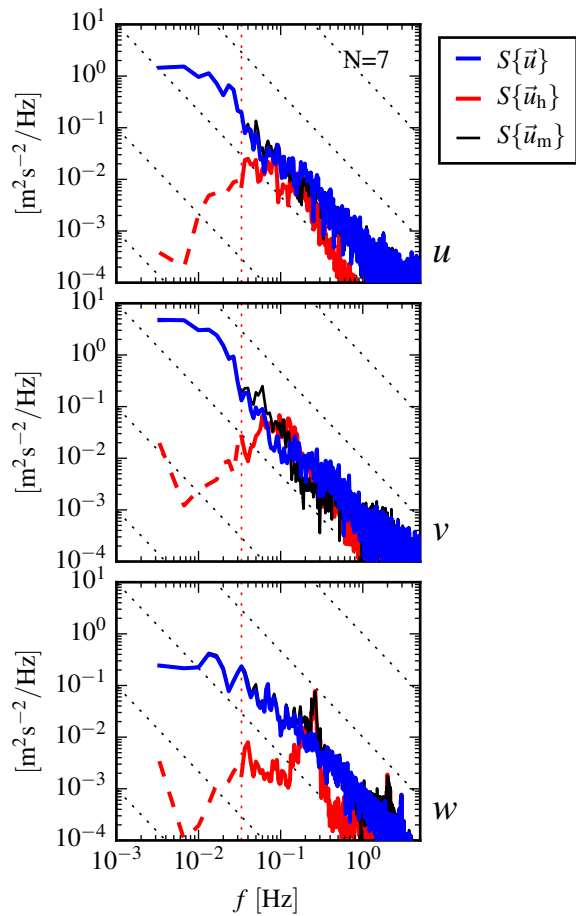
FIG. 7. Time series of tidal velocity at Admiralty Head from TTM measurements (black), and an acoustic Doppler profiler (red). The profiler measurements—taken at the same depth as the ADV on the TTM—were contaminated by acoustic reflection from the strongback fin when it was inline with one of the profiler’s beams. Note that the vertical scale on the three axes vary by more than an order of magnitude; the small ticks in A and B are equivalent to the ticks in C.



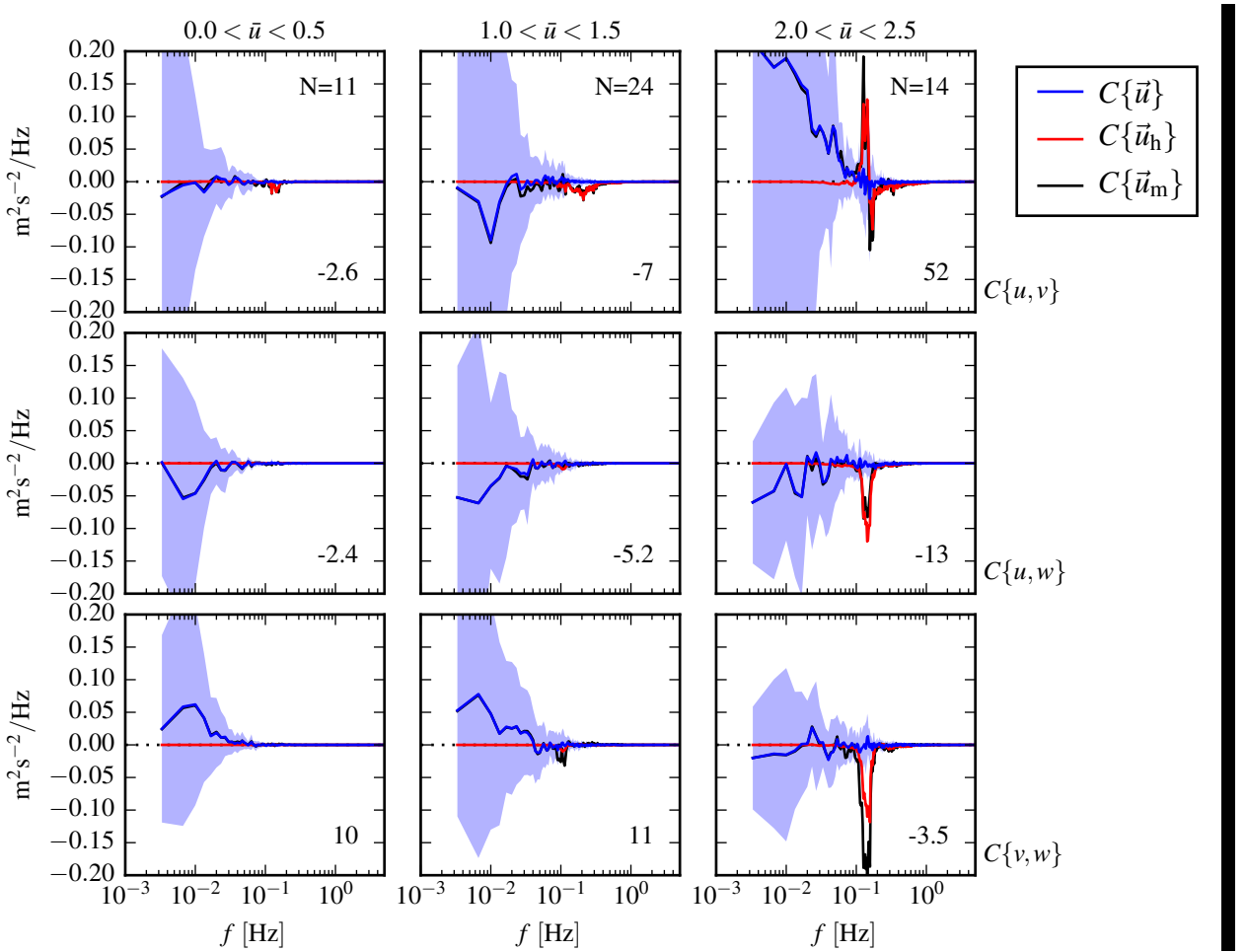
730 FIG. 8. Turbulence spectra from the June 2014 TTM deployment. Each column is for a range of streamwise  
 731 velocity magnitudes (indicated at top). The rows are for each component of velocity (indicated to the lower right  
 732 of the right column). The uncorrected spectra are in black and the corrected spectra are blue, and the spectra  
 733 of ADV head motion,  $\vec{u}_h$ , is red (also indicated in the legend). The vertical red dotted line indicates the filter  
 734 frequency applied to the IMU accelerometers when estimating  $\vec{u}_h$ ; below this frequency  $S\{\vec{u}_h\}$  is plotted as a  
 735 dashed line. Diagonal black dotted lines indicate a  $f^{-5/3}$  slope. The number of spectral ensembles, N, in each  
 736 column is indicated in the top row.



737 FIG. 9. Turbulence spectra from the StableMoor buoy. The axes layout and annotations are identical to Figure  
 738 8, except that  $S\{\vec{u}_h\}$  is plotted as a solid line at all frequencies because it is measured at all frequencies.



739 FIG. 10. Turbulence spectra from the turbulence torpedo during a 35-minute period when the mean velocity  
 740 was 1.3 m/s. Annotations and line colors are identical to Figure 8.



741 FIG. 11. The real part of the cross-spectral density between velocity components measured by the TTM. The  
 742 upper row is the  $u$ - $v$  cross-spectral density, the middle row is the  $u$ - $w$  cross-spectral density, and the bottom  
 743 row is the  $v$ - $w$  cross-spectral density. The columns are for different ranges of the stream-wise mean velocity  
 744 magnitude (indicated above the top row). The blue line is the cross spectrum between components of motion-  
 745 corrected velocity, the red line is the cross spectrum between components of head-motion, and the black line is  
 746 the cross spectrum between components of uncorrected velocity. The light blue shading indicates one standard  
 747 deviation of the  $C$  for the motion-corrected cross-spectral density.  $N$  is the number of spectral ensembles in each  
 748 column. The number in the lower-right corner of each panel is the motion-corrected Reynold's stress (integral  
 749 of the blue line) in units of  $10^{-4} \text{ m}^2 \text{s}^{-2}$ .

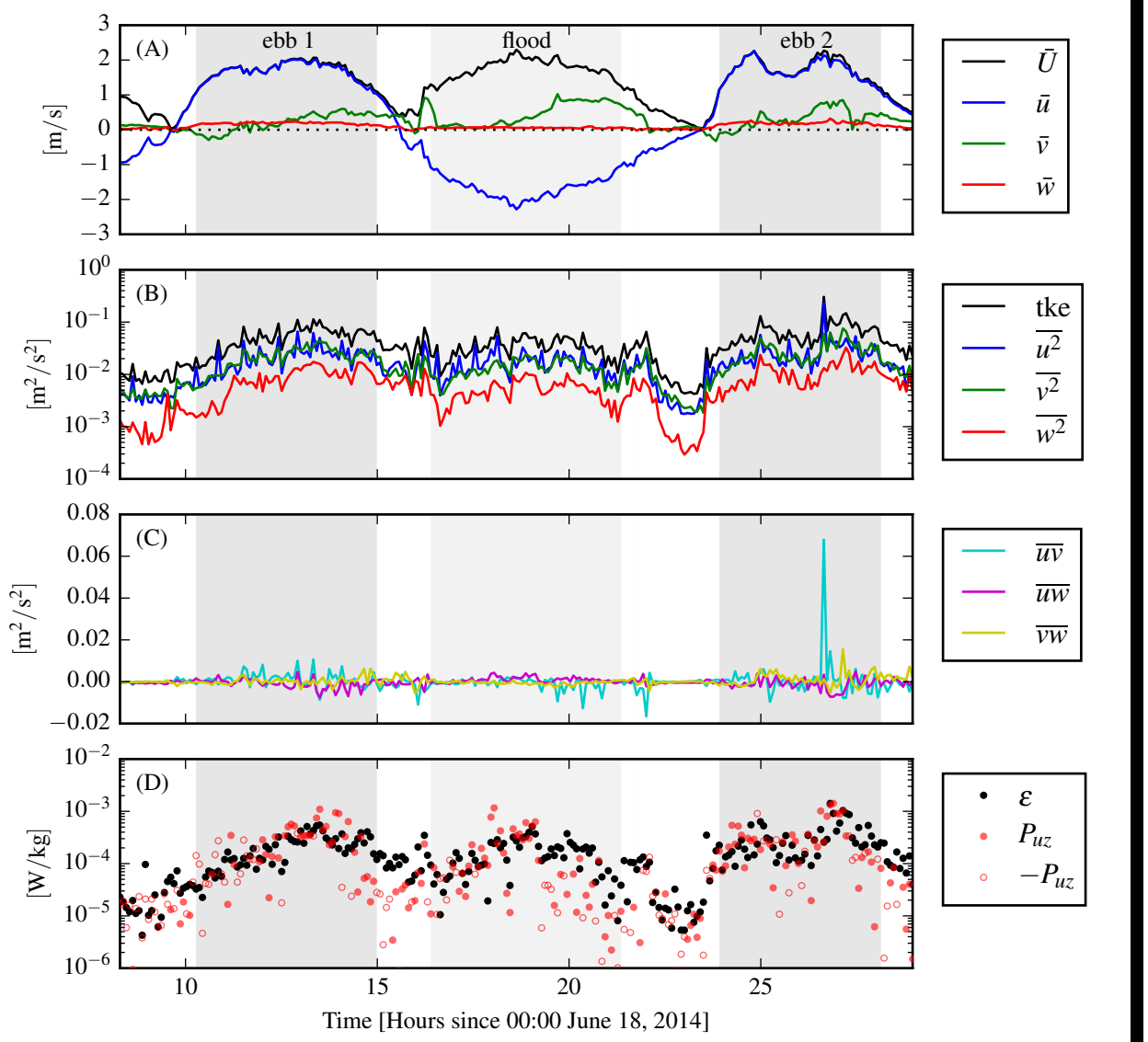
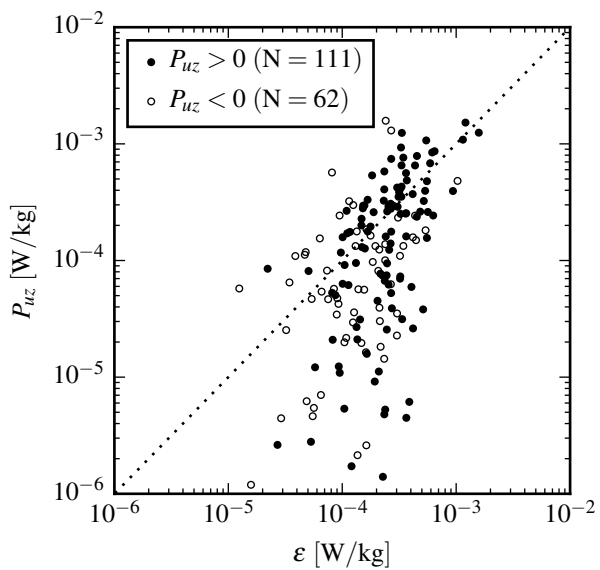
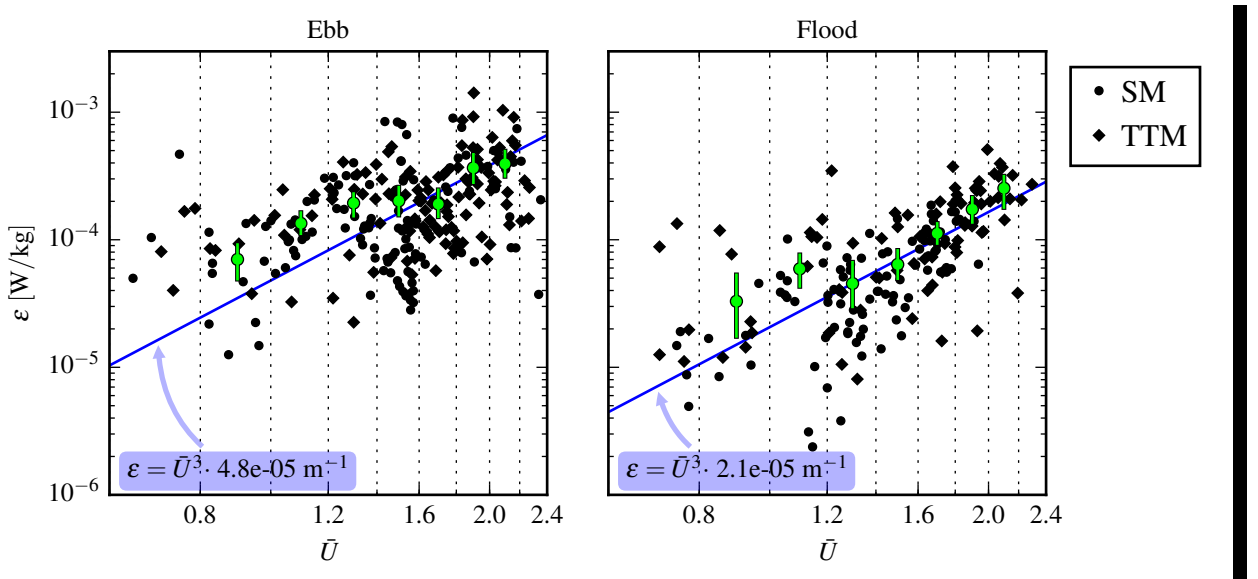


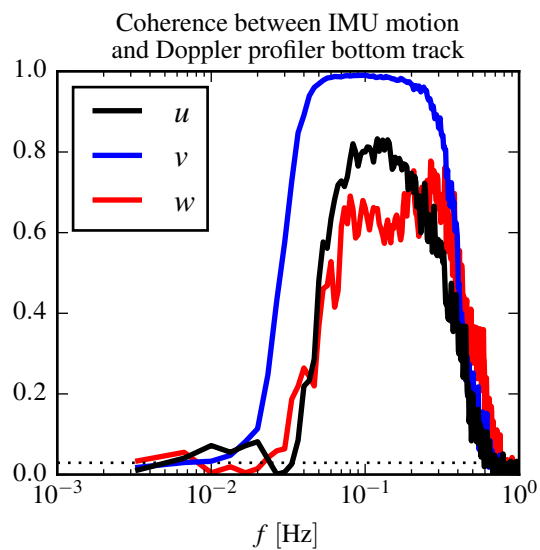
FIG. 12. Time series of mean velocities (A), turbulence energy and its components (B), Reynold's stresses (C), and turbulence dissipation rate (D) measured by the TTM during the June 2014 deployment. Shading indicates periods of ebb ( $\bar{u} > 1.0$ , grey) and flood ( $\bar{u} < -1.0$ , lighter grey).



753 FIG. 13.  $P_{uz}$  vs.  $\epsilon$  during the June 2014 TTM deployment for values of  $|u| > 1$  m/s.  
 754 Values of negative production are indicated as open circles.



755 FIG. 14. A log-log plot of  $\varepsilon$  versus  $\bar{U}$  for the June 2014 TTM (diamonds) and May 2015 StableMoor (dots)  
 756 deployments, during ebb (left) and flood (right). Black points are 5-minute averages. Green dots are mean values  
 757 within speed bins of  $0.2 \text{ m s}^{-1}$  width that have at least 10 points (50 minutes of data); their vertical bars are 95%  
 758 bootstrap confidence intervals. The blue line shows a  $U^3$  slope, wherein the proportionality constant (blue box)  
 759 is calculated by taking the log-space mean of  $\varepsilon/U^3$ .



760 FIG. 15. Coherence between IMU-measured motion of StableMoor buoy and ADP bottom-track velocity for  
 761  $1.0 < \bar{U} < 1.5$ . The horizontal dotted line indicates the 95% confidence level for the 102 spectral windows in  
 762 this estimate.